
^{18}F -FDG Small-Animal PET for Monitoring the Therapeutic Effect of CT-Guided Radiofrequency Ablation on Implanted VX2 Lung Tumors in Rabbits

Tomohisa Okuma¹, Toshiyuki Matsuoka¹, Terue Okamura², Yasuhiro Wada^{3,4}, Akira Yamamoto¹, Yoshimasa Oyama¹, Koichi Koyama¹, Kenji Nakamura¹, Yasuyoshi Watanabe^{3,4}, and Yuichi Inoue¹

¹Department of Radiology, Osaka City University Graduate School of Medicine, Osaka, Japan; ²Saiseikai Nakatsu PET Center, Osaka, Japan; ³Department of Physiology, Osaka City University Graduate School of Medicine, Osaka, Japan; and ⁴Frontier Research System, RIKEN, Tokyo, Japan

The primary goals of this study were to investigate the behavior of normal lung tissues after radiofrequency ablation (RFA) and to determine the suitability of ^{18}F -FDG PET, using a dedicated small-animal scanner, for monitoring the early therapeutic effects of RFA on VX2 lung tumors (VX2s) in rabbits. **Methods:** Fourteen Japanese white rabbits with normal lungs underwent RFA, followed by ^{18}F -FDG PET at 1 d and at 1, 2, 4, and 8 wk. In addition, 7 rabbits with untreated VX2s underwent ^{18}F -FDG PET, and 13 rabbits with RFA-treated VX2s underwent ^{18}F -FDG PET at 1 d ($n = 7$) or 1 wk ($n = 6$) after the treatment. **Results:** After RFA of normal lungs, ring-shaped accumulations of ^{18}F -FDG, which coincided with inflammation caused by ablation, were observed. The mean early- (40–60 min after injection) and delayed (100–120 min)-phase ablated lesion-to-muscle ratios were, respectively, 2.9 ± 1.0 and 3.3 ± 0.8 (1 d), 4.1 ± 0.6 and 5.2 ± 0.9 (1 wk), 4.1 ± 1.0 and 5.3 ± 1.5 (2 wk), 3.1 ± 0.5 and 3.6 ± 1.1 (4 wk), and 1.8 ± 0.1 and 2.3 ± 0.1 (8 wk). At 4 and 8 wk, the uptake was less than that at 1 and 2 wk ($P < 0.05$). VX2s showed mean tumor-to-muscle ratios of 6.6 ± 2.1 and 8.6 ± 3.3 at the early and delayed phases, respectively. For ablated tumors, the respective ratios were 0.8 ± 0.4 and 1.1 ± 0.7 (1 d) and 1.2 ± 0.5 and 1.5 ± 0.7 (1 wk). These values were significantly lower than those for nonablated tumors ($P < 0.001$). Histopathologic examination confirmed the absence of viable tumors. ^{18}F -FDG accumulation around ablated tumors reflected thermally damaged normal tissues and was significantly lower than that of control VX2s ($P < 0.01$). **Conclusion:** Our data suggest that ^{18}F -FDG PET is promising for evaluating the therapeutic response of lung malignancies to RFA: Accumulation of ^{18}F -FDG in surrounding normal tissues appears to be time dependent, and the data suggest that, clinically, ^{18}F -FDG PET should be performed 4 wk or more after RFA. Delayed-phase images seem to better distinguish tumor from inflammation than do early-phase images.

Key Words: radiofrequency ablation; microPET; lung; animal model; VX2 carcinoma

J Nucl Med 2006; 47:1351–1358

Percutaneous radiofrequency ablation (RFA) under imaging guidance is a therapeutic method that induces coagulative necrosis of targeted tissues by the application of heat through an inserted electrode needle. RFA is widely used for the treatment of hepatocellular carcinoma and metastatic liver cancer and has produced promising outcomes as a minimally invasive local control for various tumors. Several studies have reported the effectiveness of RFA for inoperative pulmonary tumors (1–11).

Recent advances in ^{18}F -FDG PET have enhanced its use for differentiating malignant from benign tumors, staging tumors, detecting metastasis, and evaluating treatment effects and relapses (12–15). In general, responses to cancer treatment manifest as local-tissue metabolic changes and circulatory changes before the appearance of morphologic alterations. ^{18}F -FDG PET, which monitors metabolic and functional changes in living individuals, can be used for the early assessment of various therapies for malignant tumors. The suitability of ^{18}F -FDG PET for evaluating RFA treatment of lung tumors has also been reported (3,4,10,11). There are, however, no established baseline data on ^{18}F -FDG accumulation early after RFA. For clinical RFA of lung tumors, the surrounding normal tissues are also ablated as a safety margin to ensure complete tumor ablation. It is possible for ablation-related inflammatory changes in normal surrounding tissues to be detected by ^{18}F -FDG PET after RFA. Thus, in the early stage, it might sometimes be difficult to determine whether the high ^{18}F -FDG accumulation reflects residual tumor or, rather, inflammatory changes due to RFA in normal surrounding tissues. It is important to distinguish thermally damaged normal tissues from residual tumor

Received Jan. 26, 2006; revision accepted Jan. 30, 2006.
For correspondence or reprints contact: Tomohisa Okuma, MD, Department of Radiology, Osaka City University Graduate School of Medicine, 1-4-3 Asahimachi, Abeno-ku, Osaka 545-8585, Japan.
E-mail: o-kuma@msic.med.osaka-cu.ac.jp
COPYRIGHT © 2006 by the Society of Nuclear Medicine, Inc.

because persistent uptake indicating the latter would require additional therapy.

In this study, we used a high-resolution dedicated small-animal PET scanner (microPET P4 [primate 4-ring]; Concord Microsystems Inc.). This scanner is currently used for the study of physiologic processes in the brain and nervous system and for molecular imaging (16,17), but its application to experimental cancer research in animals is still limited (18,19). The purpose of our study was to investigate the ^{18}F -FDG accumulation in normal lung tissues after RFA, to determine the suitability of ^{18}F -FDG PET for monitoring the early therapeutic effects of RFA on VX2 lung tumors (VX2s), and to correlate the accumulation of ^{18}F -FDG with histologic findings. We aimed to establish the optimal time at which to assess response after RFA in order to avoid ^{18}F -FDG accumulation caused by RFA-induced inflammatory changes in normal surrounding tissues.

MATERIALS AND METHODS

All experiments were conducted with the prior approval of the Laboratory Animal Center and Radioisotope Center of the Osaka City University Graduate School of Medicine. The study was conducted on Japanese white rabbits weighing 2.0–2.5 kg. All surgical procedures were conducted while the animals were under general anesthesia, as induced by intramuscular ketamine (40 mg/g) and xylazine (4 mg/kg) and maintained with a continuous infusion of ketamine (120 mg/kg/h) and xylazine (12 mg/kg/h) via an ear vein, as necessary.

Preparation of VX2 Model

Sixty rabbits were positioned supine under general anesthesia, administered as described above. Under CT guidance (ProSpeed; GE Healthcare), an 18-gauge needle was percutaneously inserted into the lung and its tip positioned in the left lower lobe. Through a 20-gauge aspiration needle placed coaxially, we slowly injected 0.4 mL of the VX2 cell suspension (8×10^6 cells). Unenhanced CT 1 wk later confirmed that tumor lesions 7–14 mm in diameter (mean, 10.5 ± 2.2 mm) had developed in 36 (60%) of the rabbits, which were used for the following experiments. Seven of these 36 rabbits later underwent ^{18}F -FDG PET without prior RFA, 13 underwent ^{18}F -FDG PET after RFA, and 16 did not undergo PET or histopathologic examination and died within 4 wk because of tumor growth, mediastinal lymph node metastasis, pleural dissemination, and malignant pleural effusion. Of the remaining 24 rabbits, which were excluded from the study, 7 showed pleural dissemination in the lung but no solid mass or distant metastases, and 17 showed no viable tumor cells at postmortem examination.

Isolation of VX2s

VX2s previously implanted and maintained in the thigh muscles of rabbits were surgically removed under general anesthesia and minced to 1-mm pieces with a pair of scissors. The pieces were filtered through a metal mesh to obtain a suspension of single tumor cells, the cells were centrifuged at 1,000 rpm for 5 min, and saline solution was added to make a suspension of approximately 2×10^7 cells/mL.

RFA

A total of 27 rabbits, 14 control rabbits with normal lungs and 13 of the VX2 rabbits, underwent RFA. Under general anesthesia,

administered as described above, a LeVeen needle electrode (RadioTherapeutics) with 10 retractable hooks having a maximum diameter of 2 cm was percutaneously inserted under CT guidance into the VX2 in the basal segment of the left lower lobe or, in control rabbits, into normal tissue in the basal segment of the right lower lobe. After having been confirmed on CT to be correctly positioned in the basal segment of the lower lobe, the needle tip was fully opened. A pair of grounding pads was taped to the (shaven) abdomen. An RF2000 generator (RadioTherapeutics) was used to create radiofrequency, which was started at 20 W, was increased to 30 W after 2 min, and was applied until automatically stopped by the increased resistance caused by so-called tissue roll-off, at which impedance reaches a maximum (20–22). After 30 s of cooling, the electric current was applied again at the same position until roll-off. Impedance and the duration of ablation were automatically recorded.

^{18}F -FDG PET

The microPET P4 system has an animal port 22 cm in diameter, an axial extent of 7.8 cm, a capacity of 63 parallel slices, a spatial resolution of 1.75 mm in full width at half maximum at the center of the field of view, a detector system composed of 32 crystal rings of lutetium oxyorthosilicate, and a 3-dimensional list-mode method of data acquisition.

The rabbits were kept fasting at least 4 h before ^{18}F -FDG PET and were scanned while they were under intravenous anesthesia. They were securely positioned prone using a handmade holding device, and transmission scanning was performed for 17 min with a $^{68}\text{Ge}/^{68}\text{Ga}$ point source for attenuation correction. ^{18}F -FDG (37 MBq/kg) was then administered via an ear vein, and emission data were acquired for the following 120 min with an energy window of 350–650 keV and a coincidence timing window of 6 ns. The transmission data were processed by μ -map calibration and segmentation (segmented attenuation correction) to obtain the attenuation correction data. The emission images were reconstructed by filtered backprojection. The raw data acquired over 120 min were divided into six 20-min frames, and data from the third and sixth frames were used to evaluate early data (40–60 min) and delayed data (100–120 min), respectively.

Two radiologists independently evaluated the ablated areas of normal lungs and the ablated untreated and RFA-treated VX2s visually and quantitatively. These radiologists were not aware of whether the ^{18}F -FDG PET images were of the early phase or the delayed phase. On visual assessment, uptake was graded on a 4-point scale in comparison with activity in back muscle: 0 = absence of uptake, 1 = faint uptake (lower than back muscle), 2 = moderate uptake (about the same as back muscle), and 3 = intense uptake.

Quantitative assessment was performed using ASIPro 4.10 software (Concord Microsystems). Circular regions of interest 2–3 mm in diameter were placed on the ^{18}F -FDG accumulation around the ablated area of normal lungs and on the untreated VX2s, as well as on ring-shaped accumulations around RFA-treated VX2s. For each image, the values of 6 regions of interest on the back muscle were averaged to produce a value for normal muscle activity, and the ratios of RFA-treated lesion to muscle (RF/M) and tumor to muscle (T/M) were calculated for the early and delayed phases. We used T/M ratio, rather than standardized uptake value (SUV), for quantitative comparison of ^{18}F -FDG uptake. The SUV was estimated to be very low, because our precedent study showed that the accumulation of ^{18}F -FDG in the stomach and intestines was much higher on whole-body small-animal PET of normal rabbits than on whole-body PET of humans.

Experimental Design

¹⁸F-FDG PET Evaluation After RFA of Normal Lungs. CT-guided RFA was performed on 14 rabbits with normal lungs, and a total of 25 PET scans (at 1 d [$n = 6$], 1 wk [$n = 6$], 2 wk [$n = 5$], 4 wk [$n = 6$], and 8 wk [$n = 2$]) were obtained. The accumulation of ¹⁸F-FDG and its time-dependent changes were compared with histopathologic findings.

¹⁸F-FDG PET Monitoring of RFA Effect on VX2s. Twenty rabbits with tumors were divided into 2 groups for the ¹⁸F-FDG PET study. The first was a control VX2 group, consisting of 7 rabbits with an untreated solitary VX2 that was evaluated by ¹⁸F-FDG PET. The second was a VX2 + RFA group, consisting of 13 rabbits with a solitary VX2 on which CT-guided RFA was performed, followed by ¹⁸F-FDG PET 1 d later in 7 rabbits and 7 d later in 6 rabbits.

Histopathologic Examination

Three, 3, 1, 4, and 2 rabbits undergoing normal-lung RFA were euthanized by an excess of ketamine and xylazine at 1 d, 1 wk, 2 wk, 4 wk, and 8 wk, respectively, after RFA. The 7 rabbits of the control VX2 group and the 13 rabbits of the VX2 + RFA group were euthanized in the same manner immediately after PET scanning. Their lungs were fixed with 10% formalin, transaxially sliced, embedded in paraffin, sectioned with a microtome, and stained with hematoxylin and eosin for histopathologic examination and for comparison with ¹⁸F-FDG PET images.

Statistical Analysis

The early- and delayed-phase T/M ratios of each group were analyzed statistically using the Wilcoxon signed-ranks test. Inter-group analysis of T/M ratios was performed using the Mann-Whitney test. Data are expressed as mean \pm SD. A P value of less than 0.05 was considered to represent a statistically significant difference.

RESULTS

¹⁸F-FDG PET Evaluation After RFA of Normal Lungs

CT-guided RFA was successfully performed on all 14 rabbits with normal lungs (Fig. 1A). Postoperative complications included pneumothorax ($n = 3$), subcutaneous emphysema ($n = 1$), and obstructive pneumonia ($n = 1$). Roll-off was reached in 187 ± 75 s, on average, in a single ablation. The mean initial impedance in normal lungs was $167.1 \pm 76.6 \Omega$.

On visual analysis, ring-shaped accumulations of ¹⁸F-FDG were found 1 d after RFA around the lesions showing less uptake (Figs. 1B and 2A). These ring-shaped accumulations were more prominent at 1 wk than at 1 d (Figs. 1C

and 2C). Similar ¹⁸F-FDG PET findings were seen after 2 wk. The accumulation of ¹⁸F-FDG was less at 4 and 8 wk than at 1 and 2 wk (Figs. 1D and 2F). The respective mean early- and delayed-phase visual scores for ¹⁸F-FDG accumulation were 1.3 ± 0.6 and 1.7 ± 0.5 (1 d, $n = 6$), 2.2 ± 0.4 and 2.2 ± 0.4 (1 wk, $n = 6$), 2.0 ± 0.0 and 2.2 ± 0.4 (2 wk, $n = 5$), 1.3 ± 0.5 and 1.5 ± 0.8 (4 wk, $n = 6$), and 1.0 ± 0.0 and 1.0 ± 0.0 (8 wk, $n = 2$). Early-phase RF/M ratios were significantly higher at 1 wk than at 1 d ($P < 0.05$) and were significantly decreased at 4 and 8 wk ($P < 0.05$) (Table 1).

On histopathologic analysis, the ring-shaped regions of high ¹⁸F-FDG uptake 1 d after RFA were found to correspond to the outer layer and consisted of vascular congestion accompanied by hemorrhage and neutrophil infiltration in the pulmonary alveoli. The low ¹⁸F-FDG accumulation inside the rings corresponded to an inner layer consisting of a coagulative necrotic lesion in which cytoplasmic eosinophilic degeneration, pyknotic nuclei, and acidophilic changes were observed (Fig. 2B).

The higher activity of ring-shaped accumulations at 1 and 2 wk appeared to reflect the outer layer of increased neutrophil infiltration and granulomatous lesions in the histopathologic specimens (Figs. 2D and 2E). At 4 and 8 wk after RFA, fibrosis of the granulomatous lesions and shrinkage of the inner necrotic lesions were observed histologically (Fig. 2G).

On quantitative analysis, the mean early- and delayed-phase RF/M ratios in the outer layer were 2.9 ± 1.0 and 3.3 ± 0.8 (1 d, $n = 6$), 4.1 ± 0.6 and 5.2 ± 0.9 (1 wk, $n = 6$), 4.1 ± 1.0 and 5.3 ± 1.5 (2 wk, $n = 5$), 3.1 ± 0.5 and 3.6 ± 1.1 (4 wk, $n = 6$), and 1.8 ± 0.1 and 2.3 ± 0.1 (8 wk, $n = 2$) (Fig. 3). Delayed-phase RF/M ratios were significantly higher than early-phase RF/M ratios at 1 d and at 1 and 2 wk after RFA ($P < 0.05$), but no statistical difference was observed at 4 and 8 wk between the early- and delayed-phase RF/M ratios. Delayed-phase RF/M ratios were significantly higher at 1 wk than at 1 d ($P < 0.05$) but were significantly decreased at 4 and 8 wk ($P < 0.05$). Delayed-phase RF/M ratios at 1 d were significantly different from those at 2 wk ($P < 0.05$). Early-phase RF/M ratios were significantly higher at 1 wk than at 1 d ($P < 0.05$) but were significantly decreased at 4 and 8 wk ($P < 0.05$). There was no statistical difference in either early- or delayed-phase RF/M ratios between 1 d and 4 wk or between 1 and 2 wk.

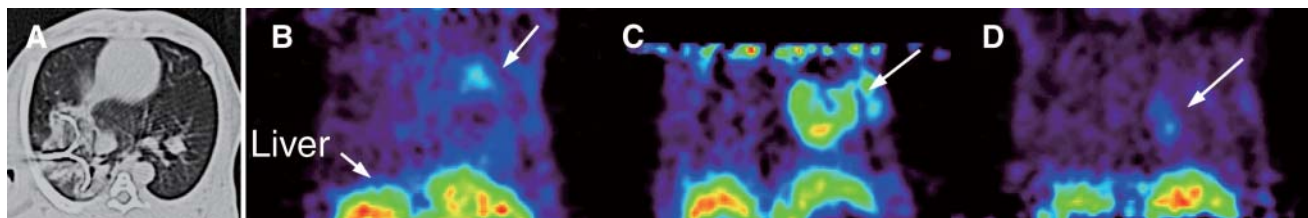


FIGURE 1. Follow-up images of normal lung after RFA over time. (A) CT image immediately after RFA shows LeVeen needle positioned in right lower lobe of lung and increased density around needle. (B) Coronal PET image 1 d after RFA shows ring-shaped accumulation of ¹⁸F-FDG (arrow) at site of RFA. (C) Coronal PET image 1 wk after RFA shows similar but higher accumulation. (D) Coronal PET image 8 wk after RFA shows reduced ¹⁸F-FDG uptake.

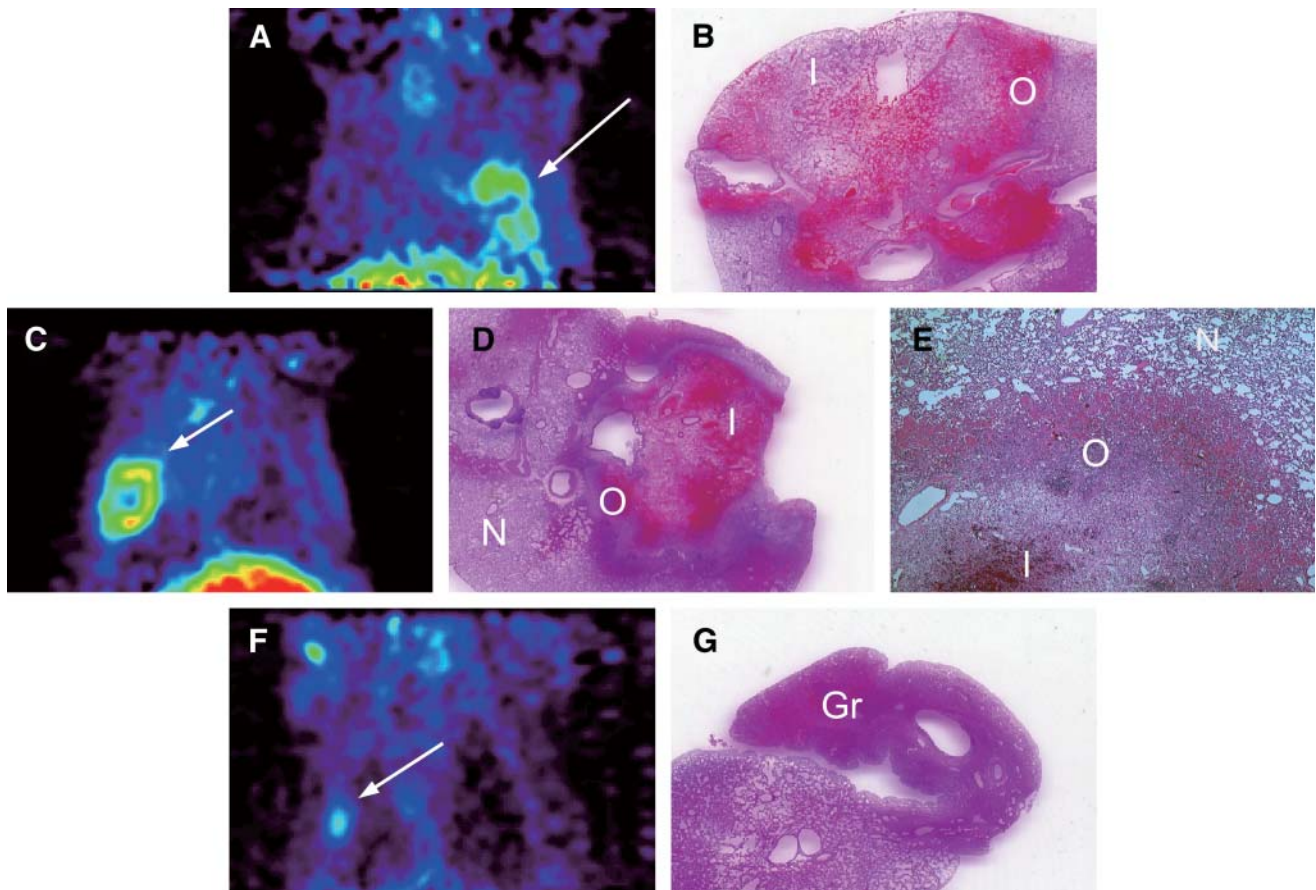


FIGURE 2. (A and B) In normal lung 1 d after RFA, coronal PET image (A) shows ring-shaped accumulation of ^{18}F -FDG (arrow) at site of RFA, and histopathologic specimen (B) shows coagulative necrosis in inner zone, relatively fewer morphologic changes in mid zone, congestion and inflammatory cell infiltration in outer zone, and an area of normal lung tissue. Region of ^{18}F -FDG accumulation on PET correlates with outer layer of inflammatory cell infiltration. (C–E) One week after RFA, coronal PET image (C) shows an accumulation similar to but higher than that at 1 d, and histopathologic specimens (normal view [D] and magnified view [$\times 40$, E]) show increasing inflammatory cell infiltration and granulomatous changes in outer and inner zones and an area of normal lung tissue. (F and G) Four weeks after RFA, coronal PET image (F) shows reduced ^{18}F -FDG uptake, and histopathologic specimen (G) shows granulomatous tissues, fibrosis, and inner necrotic regions reduced in size. Gr = granulomatous tissues; I = inner zone; N = normal tissue; O = outer zone.

^{18}F -FDG PET Monitoring of RFA Effect on VX2s

Control VX2 Group. On visual analysis, a high accumulation of ^{18}F -FDG was observed in all 7 rabbits with a solitary, untreated VX2 (Fig. 4A). The mean early- and delayed-phase visual scores were 2.9 ± 0.4 and 2.9 ± 0.4 , respectively.

On quantitative analysis, the mean T/M ratios of the tumors were 6.6 ± 2.1 and 8.6 ± 3.3 at the early and delayed phases, respectively. The delayed-phase T/M ratio was significantly higher than the early-phase T/M ratio ($P < 0.001$). Histopathologically, the ^{18}F -FDG accumulations correlated with viable VX2 cells (Fig. 4B).

VX2 + RFA Group. CT-guided RFA was successfully performed on all 13 rabbits of the VX2 + RFA group (Figs. 4C and 4D). Mild pneumothorax occurred in 2 cases. The mean ablation time until roll-off was 296 ± 107 s. The mean initial impedance of VX2s was $105.9 \pm 34.1 \Omega$.

On visual analysis, the PET images showed low accumulations of ^{18}F -FDG surrounded by regions of ring-shaped

high ^{18}F -FDG uptake (Fig. 5A). Similar findings were seen at 1 wk. The visual scores are summarized in Table 1.

On histopathologic analysis, characteristics of ongoing necrosis were seen: blurred cytoplasmic borders, eosinophilic degeneration in the cytoplasm, pyknotic nuclei, and blurred chromatin by hematoxylin and eosin staining (Figs. 5B and 5C). Histopathologic examination at 1 d and 1 wk after RFA confirmed the absence of viable tumor and the absence of local recurrence at the edge of the ablated lesions. As in normal lung tissues treated with RFA, a surrounding area of high ^{18}F -FDG uptake at 1 d coincided with inflammatory changes in the histopathologic specimen, that is, exudative inflammation, congestion, and hemorrhage in the alveoli at the outer layer. Histopathologic findings at 1 wk after RFA showed an outer layer of increased neutrophil infiltration and granulomatous lesions.

On quantitative analysis, the mean early- and delayed-phase T/M ratios were 0.8 ± 0.4 and 1.1 ± 0.7 , respectively, at 1 d after RFA ($n = 7$) (Fig. 6) and 1.2 ± 0.5 and 1.5 ± 0.7 ,

TABLE 1

Comparison of Visual and Quantitative Results and Histopathologic Findings at Various Times of Sacrifice

Time of sacrifice	Visual score	Ratio*		Histopathologic findings
		Early	Delayed	
RFA-treated normal-lung groups				
1 d	1.3 ± 0.6	2.9 ± 1.0	3.3 ± 0.8	Inflammation, congestion, and hemorrhage
1 wk	2.2 ± 0.3	4.1 ± 0.6	5.2 ± 0.9	Marked infiltration of neutrophils
2 wk	2.0 ± 0.0	4.1 ± 1.0	5.3 ± 1.5	Inflammatory changes (same as at 1 wk)
4 wk	1.3 ± 0.5	3.1 ± 0.5	3.6 ± 1.1	Fibrosis of granulomatous changes
8 wk	1.0 ± 0.0	1.8 ± 0.1	2.3 ± 0.1	Small granulation; size reduction of necrotic lesions
VX2 groups				
Without RFA	2.9 ± 0.4	6.6 ± 2.1	8.6 ± 3.3	Viable VX2 cells
With RFA (ablated tumor), 1 d	0.3 ± 0.5	0.8 ± 0.4	1.1 ± 0.7	Ongoing necrosis of tumor cells
With RFA (outer zone), 1 d	1.3 ± 0.5	3.5 ± 0.9	4.4 ± 1.2	Inflammation, congestion, and hemorrhage
With RFA (ablated tumor), 1 wk	0.4 ± 0.5	1.2 ± 0.5	1.5 ± 0.7	Ongoing necrosis of tumor cells
With RFA (outer zone), 1 wk	1.7 ± 0.5	3.9 ± 0.7	4.7 ± 1.1	Strong infiltration of neutrophils

*Data are RF/M for RFA-treated normal-lung groups and T/M for VX2 groups.

respectively, at 1 wk ($n = 6$). The T/M ratios for the early and delayed phases at 1 d did not significantly differ from those at 1 wk ($P = 0.57$ and 0.48 for the early and delayed phases, respectively).

At the ring-shaped area of uptake in the outer layer, the mean early- and delayed-phase RF/M ratios were 3.5 ± 0.9 and 4.4 ± 1.2 at 1 d and 3.9 ± 0.7 and 4.7 ± 1.1 at 1 wk, and the delayed-phase RF/M ratios were significantly higher than the early-phase RF/M ratios at both 1 d and 1 wk ($P < 0.05$).

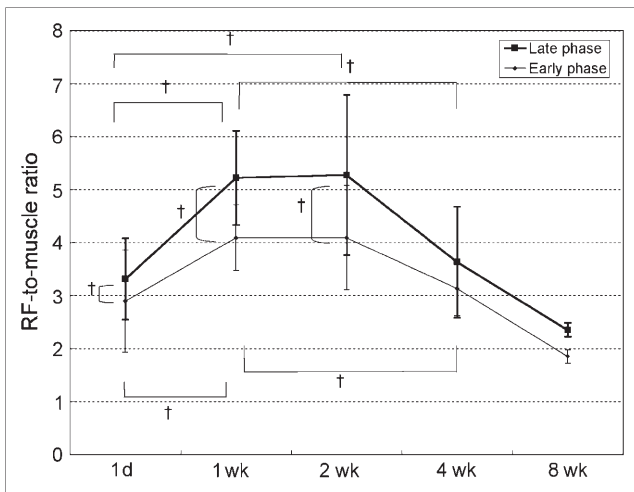


FIGURE 3. Graph showing time-dependent changes in ^{18}F -FDG accumulation in normal lungs after RFA, as reflected by changes in early- and delayed-phase RF/M ratios. ^{18}F -FDG uptake was highest at 1 and 2 wk, with a significantly higher RF/M ratio at 1 wk than at 1 d. RF/M ratio was significantly lower after 4 and 8 wk than at 1 wk. These changes corresponded to the histologic changes shown in Figure 2. Up until 2 wk, delayed-phase RF/M ratios remained significantly higher than early-phase RF/M ratios, indicating strong inflammatory responses. After 4 wk, there was no statistical difference between early- and delayed-phase RF/M ratios. † $P < 0.05$.

These ratios were close to the ratio observed in normal lungs after RFA.

Intergroup Comparisons. Significant differences in both the early-phase and the delayed-phase T/M ratios were found between the control VX2 group and the VX2 + RFA group at 1 d after RFA and between the control VX2 group and the VX2 + RFA group at 1 wk after RFA ($P < 0.001$). Both the early-phase and the delayed-phase RF/M ratios in the outer layer were significantly higher at 1 d and 1 wk after RFA ($P < 0.05$). Both the early-phase and the delayed-phase RF/M ratios in the outer layer were significantly lower in control VX2s ($P < 0.01$).

DISCUSSION

Since the first clinical trial of RFA in 3 patients with lung tumors by Dupuy et al. in 2000 (3), other groups have also reported the effectiveness of CT-guided RFA for the treatment of lung malignancies in patients who cannot be treated by surgery or chemotherapy because either they refuse the treatment or their clinical status precludes it (3–11). The effects of RFA on normal lung tissues have been examined in animals (21–24) using MRI and CT, with special emphasis on anatomic changes in ablated lesions, but not using ^{18}F -FDG PET. CT is currently used to evaluate the response after RFA (3–11) but is limited.

Several authors have suggested that ^{18}F -FDG PET may be useful for evaluating the outcome of RFA treatment of early-stage lung lesions (3,4,10,11), but their reports were based on few clinical cases.

In this study, we used a high-resolution dedicated small-animal PET scanner to examine the degree and time dependency of changes in ^{18}F -FDG uptake in normal rabbit-lung tissues during the inflammatory response to thermal injury caused by RFA. The ring-shaped ^{18}F -FDG accumulation that we observed 1 d after RFA of normal lung tissues corresponded to the histopathologically observed inflammatory

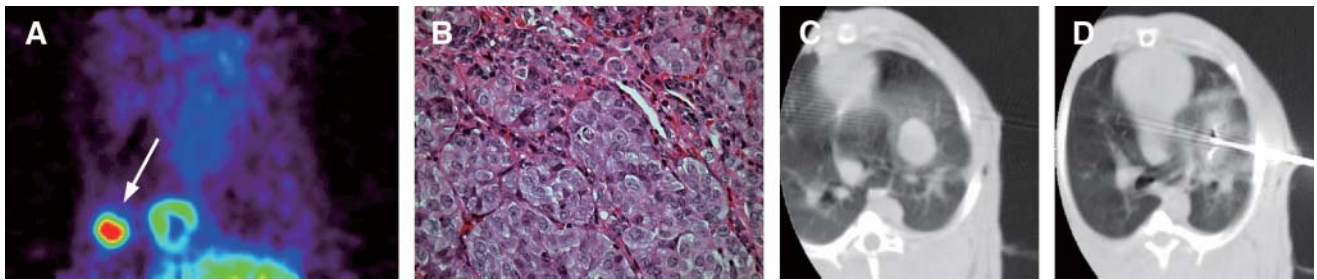


FIGURE 4. (A and B) In representative rabbit with untreated VX2, coronal PET image (A) shows extensive ^{18}F -FDG uptake (arrow) in VX2, and histopathologic specimen ($\times 400$, B) shows tumor cells with high nuclear-to-cytoplasmic ratio and abnormal nuclear morphology. (C and D) In representative rabbit with RFA-treated VX2, CT image before treatment (C) shows round tumor with clear boundary, and CT image immediately after treatment (D), with LeVein needle still inserted in tumor, shows increased density around tumor.

cell infiltration induced by thermal ablation. This accumulation was significantly higher at 1 and 2 wk than at 1 d and was significantly lower at 4 and 8 wk than at 1 wk. At 1 d, 1 wk, and 2 wk after RFA, the inflammatory response resulted in a significantly higher ^{18}F -FDG accumulation on delayed-phase scanning than on early-phase scanning. The ring-shaped ^{18}F -FDG accumulation was reduced at 4 and 8 wk after RFA, with no significant difference between the early and delayed phases.

A transient increase in ^{18}F -FDG accumulation due to inflammatory responses occurs during the first several weeks of radiation therapy and for 4–6 wk after chemotherapy, making evaluation of therapeutic response by ^{18}F -FDG PET less reliable. Currently, it is recommended that ^{18}F -FDG PET not be used to evaluate the effects of radiation therapy until 4–6 mo after the therapy (13,14). For clinical RFA of lung carcinoma, surrounding normal tissues are also ablated as a safety margin to eliminate cancerous cells. Thus, in the early recovery stages after RFA, inflammatory responses in the ablated normal tissues may cause an increased accumulation of ^{18}F -FDG. When ^{18}F -FDG PET is used to evaluate the therapeutic outcome of RFA of lung malignancies, it is clinically desirable to delay the examination until 4 wk or more after the treatment. A high accumulation of ^{18}F -FDG at 4 wk or later may be misinterpreted as indicating residual tumor.

In this study, we also included ^{18}F -FDG PET after RFA of VX2s. The implanted VX2 cells became viable and formed tumors in 60% of the rabbits. In 3 other studies on RFA of experimentally induced VX2s in rabbits, the rates

of successful generation of solitary VX2s were 46% (11/24), 75% (18/24), and 77.8% (34/45) (25–27). In those 3 studies, CT and MRI were used to follow the changes in ablated tumors, and the results were compared with the pathologic findings (25–27). To our knowledge, however, no studies have used ^{18}F -FDG PET to evaluate RFA of lung tumors.

On ^{18}F -FDG PET at 1 d and 1 wk after RFA of VX2s, the T/M ratios of the ablated tumors were significantly lower than the T/M ratios of nonablated tumors in the control VX2 group. Ablated lesions with a low ^{18}F -FDG accumulation corresponded histopathologically to cells showing characteristic signs of ongoing necrosis and confirmed the absence of viable tumor, suggesting the suitability of ^{18}F -FDG PET for the early evaluation of RFA outcome. The ring-shaped accumulations of ^{18}F -FDG noted around ablated VX2s reflected thermal injury to normal lung tissues. In this VX2 model, it would not be difficult to differentiate residual tumor from inflammatory changes, because the RF/M ratios of the ring-shaped accumulations were significantly lower than those of the control VX2 group. In clinical practice, however, the degree of malignancy may be diverse in primary lung tumors or lung metastases, and ^{18}F -FDG uptake would vary from mild to marked. When ^{18}F -FDG accumulation is mild to moderate, it may not be possible to determine whether residual tumor is present. In such cases, delayed-phase images would be helpful, because residual tumor may be expected to show a greater increase in activity on delayed images than on early images.

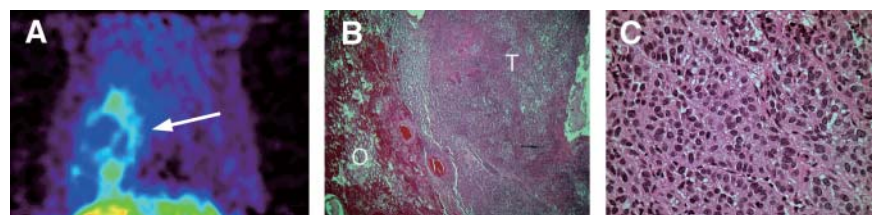


FIGURE 5. (A and B) One day after RFA, coronal PET image (A) shows completely ablated VX2 and ring-shaped accumulation of ^{18}F -FDG (arrow) around site of RFA. Histopathologic specimen ($\times 40$, B) shows VX2 necrosis and outer-zone tissue congestion and inflammatory cell infiltration. Comparison with PET image indicates that inner necrotic zone corresponds to ablated tumor mass, whereas outer inflammatory layer corresponds to ring-shaped ^{18}F -FDG accumulation. (C) High-power ($\times 400$) view of histopathologic specimen shows blurred cytoplasmic borders, pyknotic nuclei, and blurred chromatin—characteristic features of ongoing necrosis. O = outer zone; T = VX2.

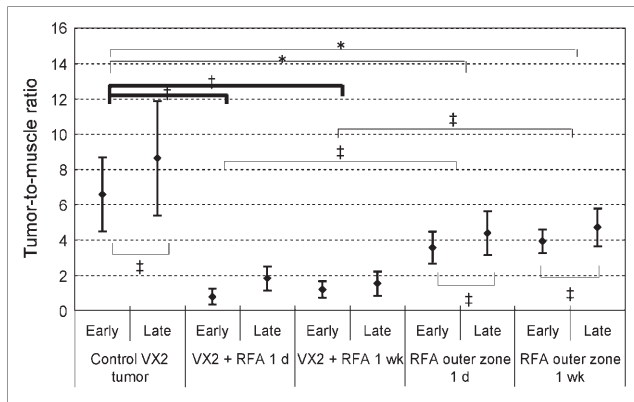


FIGURE 6. Graph comparing early- and delayed-phase T/M ratios in treated and untreated VX2s. T/M ratios of RFA-treated VX2s at 1 d and 1 wk are significantly different from those of untreated VX2s on both early-phase and delayed-phase scanning ($*P < 0.001$). Outer-layer T/M ratios of tissues surrounding treated VX2s at 1 d and 1 wk are significantly different from those of untreated VX2s on both early-phase and delayed-phase scanning ($†P < 0.01$). Outer-layer T/M ratios of tissues surrounding treated VX2s at 1 d and 1 wk are also significantly different from those of treated VX2s on both early-phase and delayed-phase scanning ($‡P < 0.05$). In treated VX2s, T/M ratios at early phase do not significantly differ from those at delayed phase ($P = 0.57$ and 0.48 , respectively), but in untreated VX2s and outer layer, which correlated with ring-shaped ^{18}F -FDG accumulation, T/M ratios are higher on delayed-phase images than on early-phase images at both 1 d and 1 wk ($‡P < 0.05$).

A limitation of our study was that RFA was performed on rabbits with normal lungs and not on humans with lung tumors. The accumulation of ^{18}F -FDG after RFA may differ between the two. Nevertheless, we believe that RFA-induced inflammatory changes in normal lung tissues surrounding lung tumors would yield similar results, with ^{18}F -FDG uptake in thermally damaged tissues appearing at 1 and 2 wk after RFA and decreasing at 4 wk or later. Another limitation of our study was that VX2s consist of biologically highly malignant cells (25–28). In our study, long-term monitoring was not possible because the local implantation of these tumor cells resulted in pleural dissemination and lymphatic metastasis. Tumor cells were initially implanted using CT-guided puncture through a coaxially inserted needle, but pleural dissemination was difficult to prevent, partly because the cells were prepared as a suspension. All rabbits that did not undergo PET died within 4 wk. Pleural dissemination occurred in 4 rabbits of the VX2 + RFA (1 wk) group. Coagulative necrosis was observed in these RFA-treated tumor lesions, and extensive malignant pleural effusion, pleural dissemination, and numerous mediastinal lymph node metastases were found at necropsy. Another limitation concerns the technical aspects of PET. In our institution, transfer of animals outside the radioisotope facility is prohibited within the first week after ^{18}F -FDG administration. Because the CT system is located outside the radioisotope facility for RFA, we could not perform CT of VX2s

after ^{18}F -FDG PET scanning, and PET after RFA of VX2s was performed using separate groups.

CONCLUSION

Although our study had some limitations, our data suggest that ^{18}F -FDG PET is promising for evaluating the therapeutic response of lung malignancies to RFA: The accumulation of ^{18}F -FDG in surrounding normal tissues appears to be time dependent, and the data suggest that, clinically, ^{18}F -FDG PET should be performed 4 wk or more after RFA. When an early-phase image (40–60 min) shows an inconclusive accumulation of ^{18}F -FDG in or surrounding an ablated area, and uptake is not significantly greater on a delayed-phase image (100–120 min) than on the early-phase image, the increased ^{18}F -FDG uptake likely indicates an inflammatory change rather than residual or recurrent tumor.

REFERENCES

- Dupuy DE, Goldberg SN. Image-guided radiofrequency tumor ablation: challenges and opportunities—part 2. *J Vasc Interv Radiol.* 2001;12:1135–1148.
- Gazelle GS, Goldberg SN, Solbiati L, Livraghi T. Tumor ablation with radiofrequency energy. *Radiology.* 2000;217:633–646.
- Dupuy DE, Zagoria RJ, Akerley W, et al. Percutaneous radiofrequency ablation of malignancies in the lung. *AJR.* 2000;174:57–59.
- Steinke K, Habicht JM, Thomsen S, et al. CT-guided radiofrequency ablation of a pulmonary metastasis followed by surgical resection. *Cardiovasc Intervent Radiol.* 2002;25:543–546.
- Suh RD, Wallace AB, Sheehan RE, et al. Unresectable pulmonary malignancies: CT-guided percutaneous radiofrequency ablation—preliminary results. *Radiology.* 2003;229:821–829.
- Herrera LJ, Fernando HC, Perry Y, et al. Radiofrequency ablation of pulmonary tumors in nonsurgical candidates. *J Thorac Cardiovasc Surg.* 2003;125:929–937.
- Nishida T, Inoue K, Kawata Y, et al. Percutaneous radiofrequency ablation of lung neoplasms: a minimally invasive strategy for inoperable patients. *J Am Coll Surg.* 2002;195:426–430.
- Yasui K, Kanazawa S, Sano Y, et al. Thoracic tumors treated with CT-guided radiofrequency ablation: initial experience. *Radiology.* 2004;231:850–857.
- Lee JM, Jin GY, Goldberg SN, et al. Percutaneous radiofrequency ablation for inoperable non-small cell lung cancer and metastases: preliminary report. *Radiology.* 2004;230:125–134.
- Akeboshi M, Yamakado K, Nakatsuka A, et al. Percutaneous radiofrequency ablation of lung neoplasms: initial therapeutic response. *J Vasc Interv Radiol.* 2004;15:463–470.
- Okuma T, Okamura T, Matsuoka T, et al. Fluorine-18-fluorodeoxyglucose positron emission tomography for assessment of patients with unresectable recurrent or metastatic lung cancers after CT-guided radiofrequency ablation: preliminary results. *Ann Nucl Med.* 2006;20:115–121.
- Herder GJ, Golding RP, Hoekstra OS, et al. The performance of fluorine-18-fluorodeoxyglucose positron emission tomography in small solitary pulmonary nodules. *Eur J Nucl Med Mol Imaging.* 2004;31:1231–1236.
- Giannopoulou C. The role of SPET and PET in monitoring tumour response to therapy. *Eur J Nucl Med Mol Imaging.* 2003;30:1173–1200.
- Kostakoglu L, Goldsmith SJ. ^{18}F -FDG PET evaluation of the response to therapy for lymphoma and for breast, lung, and colorectal carcinoma. *J Nucl Med.* 2003;44:224–239.
- Kubota K, Itoh M, Ozaki K, et al. Advantage of delayed whole-body FDG-PET imaging for tumour detection. *Eur J Nucl Med.* 2001;28:696–703.
- Cherry SR, Shao Y, Silverman RW, et al. MicroPET: a high resolution PET scanner for imaging small animals. *IEEE Trans Nucl Sci.* 1997;44:1161–1166.
- Wada Y, Matsumura A, Nakamura F, et al. Performance evaluation of microPET P4 for rat, rabbit and monkey. *Int Congr Ser.* 2004;1265:69–73.
- Kondo S, Hosono NM, Wada Y, et al. Use of FDG-microPET for detection of small nodules in a rabbit model of pulmonary metastatic cancer. *Ann Nucl Med.* 2004;18:51–57.

19. Ishii K, Hosono MN, Wada Y, et al. Usefulness of FDG-microPET for early evaluation of therapeutic effects on VX2 rabbit carcinoma. *Ann Nucl Med*. 2006;20:123–130.
20. Matsuoka T, Toyoshima M, Yamamoto A, et al. Percutaneous radiofrequency ablation for lung tumors. *Jpn J Intervent Radiol*. 2002;17:327–334.
21. Oyama Y, Nakamura K, Matsuoka T, et al. Radiofrequency ablated lesion in the normal porcine lung: long-term follow-up with MRI and pathology. *Cardiovasc Intervent Radiol*. 2005;28:346–353.
22. Yamamoto A, Nakamura K, Matsuoka T, et al. Ablation in a porcine lung model: correlation between CT and histopathological findings. *AJR*. 2005;185:1299–1306.
23. Goldberg SN, Gazelle GS, Compton CC, McLoud TC. Radiofrequency tissue ablation in the rabbit lung: efficacy and complications. *Acad Radiol*. 1995;2:776–784.
24. Wacker FK, Nour SG, Eisenberg R, Duerk JL, Lewin JS. MRI-guided radiofrequency thermal ablation of normal lung tissue: in vivo study in a rabbit model. *AJR*. 2004;183:599–603.
25. Goldberg SN, Gazelle GS, Compton CC, Mueller PR, McLoud TC. Radiofrequency tissue ablation of VX2 tumor nodules in the rabbit lung. *Acad Radiol*. 1996;3:929–935.
26. Miao Y, Ni Y, Bosmans H, et al. Radiofrequency ablation for eradication of pulmonary tumor in rabbits. *J Surg Res*. 2001;99:265–271.
27. Lee JM, Jin GY, Li CA, et al. Percutaneous radiofrequency thermal ablation of lung VX2 tumors in a rabbit model using a cooled tip-electrode: feasibility, safety, and effectiveness. *Invest Radiol*. 2003;38:129–139.
28. Oya N, Nagata Y, Tamaki N, et al. FDG-PET evaluation of therapeutic effects on VX2 liver tumor. *J Nucl Med*. 1996;37:296–302.